www.aem-iournal.com

Prototyping of Superhydrophobic Surfaces from Structure-Tunable Micropillar Arrays Using Visible Light Photocuring

Hansheng Li, Fu-Hao Chen, Saeid Biria, and Ian D. Hosein*

A new approach is reported to fabricate micropillar arrays on transparent surfaces by employing the light-induced self-writing technique. A periodic array of microscale optical beams is transmitted through a thin film of photocrosslinking acrylate resin. Each beam undergoes self-lensing associated to photopolymerization-induced changes in the refractive index of the medium, which counters the beam's natural tendency to diverge over space. As a result, a microscale pillar grows along each beam's propagation path. Concurrent, parallel self-writing of micropillars leads to the prototyping of micropillar-based arrays, with the capability to precisely vary the pillar diameter and inter-spacing. The arrays are spray coated with a thin layer of polytetrafluoroethylene (PTFE) nanoparticles to create large-area superhydrophobic surfaces with water contact angles greater than 150° and low contact angle hysteresis. High transparency is achieved over the entire range of micropillar arrays explored. The arrays are also mechanically durable and robust against abrasion. This is a scalable, straightforward approach toward structure-tunable micropillar arrays for functional surfaces and anti-wetting applications.

1. Introduction

The functional wetting properties observed in living systems^[1] has driven researchers to create biomimetic designs, toward critical applications in anti-wetting,^[2] water collection,^[3] anti-fogging,^[4] anti-corrosion, anti-icing,^[4,5] self-healing,^[6] and cell adhesion.^[7] Liquid wetting over a solid surface depends on its chemical properties and roughness, two principles that have informed the fabrication of a variety of roughened and textured surface structures.^[8] One common, reliable surface structure employed extensively in studies and applications is a periodic array of micropillars. Such pillars provide the necessary microscopic surface roughness to induce hydrophobicity that may be further enhanced through coatings or functionalization.^[8] Micropillar arrays have thus far been fabricated using soft lithography,^[2,9] etching,^[10] and photopolymerization.^[11] While significant

Prof. I.D. Hosein, H. Li, F. Chen, S. Biria Department of Biomedical and Chemical Engineering Syracuse University 130 Smith Drive, 329 Link Hall, Syracuse, New York 13244, USA E-mail: idhosein@syr.edu

DOI: 10.1002/adem.201801150

progress has been made using such techniques, all entail several steps in the fabrication process, which are often costly and time-consuming, and pose challenges with scale up toward large-area surface coatings. A more straightforward, and scalable technique is desirable to prototype and deploy micropillar array surface structures.

An alternative process to create the micropillar geometry is through light-induced self-writing (LISW).[12] The technique employs a microscale optical beam that can initiate curing to form a solid "rod"shaped polymer when transmitted through a photoreactive monomer liquid. [12a,12b,13]^[12a,12c,14,15] This occurs by beam-induced self-focusing[12a] beginning at the front of the medium by an initial layer of polymer that cures in the shape of a lens. Consequently, light is focused onto the furthest end of the polymer, and a rod shape emerges. $[12a,12c,14]^{[12a,12c,14,15]}$ This rod behaves like a small fiber-optic that channels light to its furthest tip, thereby sustaining its own growth. [12a,12c,14,15] An array of trans-

mitted beams can be generated by transmitting a wide-area light source through a photomask consisting of apertures (i.e., holes), enabling parallel writing to create a large-area array of aligned rods. [16] This process has thus far been exploited to prototype 3D materials.[15a,17][11] When oriented and deposited onto a surface, the array would assume the desired micropillar surface structure. Jun and co-workers have employed a micro-lens array, wherein passive focusing of light drove the growth of pillars. [11] Distinctly, in the LISW technique, active focusing of the optical beam is selfinduced, elicited by the inherent photopolymerization-induced changes in the refractive index, obviating any need for a micro-lens array, which is an advantage of the proposed approach. All that is required is a photomask to generate an array of microscale optical beams. Visible light photocuring of a liquid resin is straightforward and includes similar steps as in lithography, and when combined with the self-trapping process it provides the benefits of precision found in lithography. Hence, leveraging this technique to form micro-pillar arrays would demonstrate an alternative approach to generate anti-wetting surfaces.

Herein, we describe a straightforward two-step approach to fabricate superhydrophobic micropillar array surface structures on a transparent substrate using light-induced self-writing in a thin-film of photo-crosslinking resin that is sensitized to visible



(blue) light. We generate the periodic array of optical beams, which will induce self-writing, from a blue light-emitting diode (LED). Visible light irradiation is attractive owing to its low cost, scalability, and safety. Ours and other's work have demonstrated the ability to elicit self-focusing using incoherent, visible light in photopolymerizable media. [18] Herein, we tune the array structure through variation of the photomask pattern, which generates the array of optical beams with different diameters and spacings. The micropillar arrays are converted to superhydrophobic surfaces via coverage with a thin, spray-coated layer of polytetrafluoroethylene (PTFE) nanoparticles, which is an effective, scalable method to advance anti-wetting properties. [2a,19] Irregardless of micropillar diameter and inter-spacing, all structures attain superhydrophobicity and low contact angle hysteresis, demonstrating a structure-tunable, versatile technique toward anti-wetting surfaces. The transparency of the structures makes them potential candidates for applications in non-stick coatings, adhesives, windows, solar panels, safety goggles, and optical devices. This is the first demonstration of employing light-induced self-writing for scalable, straightforward fabrication of superhydrophobic surfaces, and is an attractive alternative over conventional methods investigated thus far. The novelty and significance of this work are in prototyping superhydrophobic surfaces using visible light photocuring, the versatility in the range of structures that can be produced and show superhydrophobicity, the inherent transparency of the structures, as well as the generalized nature of the process (i.e., any photoinitiated polymer system is suitable).

2. Results

Figure 1 shows a schematic of the process to fabricate micropillar arrays. The resin is irradiated by LED light that is transformed into a periodic array of microscale optical beams using a photomask consisting of an array of apertures with a

specific size and interspacing. Each microscale optical beam will undergo self-focusing owing to photopolymerizationinduced changes in the refractive index. As a result, a structure with a lens-like geometry will begin to cure and solidify at the substrate surface, and a pillar then continues to grow outward along the propagation path of the optical beam. The masks used herein are the inverse of those employed in our previous work (i.e., chrome circles and transparent surroundings) for which microscale pores were formed^[20]; whereas herein pillars are formed. We selected a mask of square geometry for simplicity in characterizing the structure, and square symmetries are common when architecting pillar arrays for anti-wetting applications. Arrays may be grown with any geometry and symmetry desired by changing the arrangement of the apertures. In this work, we employed a commercially available photo-crosslinking acrylate monomer, TMPTA, for which we have demonstrated the ability to elicit self-focusing and self-writing in its pure form,[17c] formulations, [18a] and blends, [21] After irradiation, washing away of excess monomer leaves the photocured micropillars adhered to the transparent substrate. The pillar's surface properties are then changed via spray coating a thin layer of PTFE nanoparticles. The irradiation process takes ≈20 min. to attain free-standing pillars, followed by washing then spray coating, leading to a reasonably efficient time to prototype anti-wetting surfaces. With our 2" diameter LED sources, we fabricated micropillar array structures over the same area. Scale-up is possible using larger visible light sources (i.e., LED arrays, white light lamps). Or, large-scale surfaces may be created from the assembly of "tiles" of smaller units of photocured arrays. The mask patterns were selected to achieve D:S ratios of 1:5, 1:10, and \approx 1:2, as similarly employed in previous works on micropillar arrays for anti-wetting applications.

Figure 2 presents exemplary SEM images of the micropillar arrays produced using the LISW technique over the range of mask patterns investigated. Individual pillars are formed over

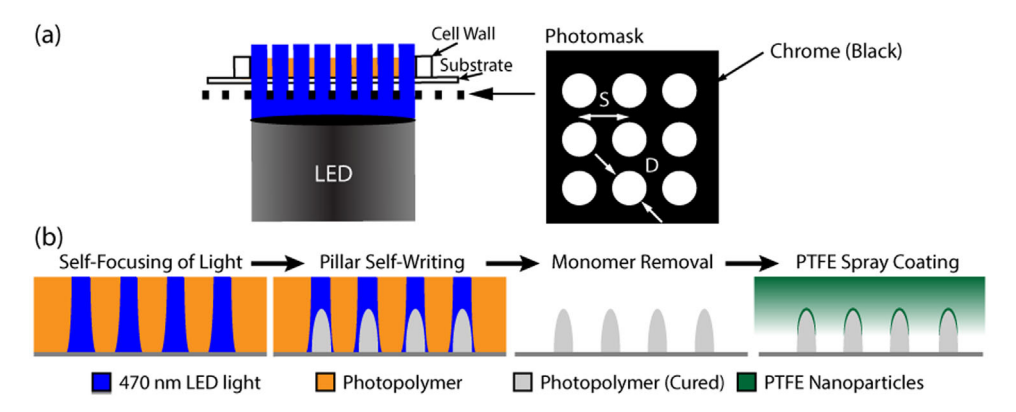


Figure 1. Procedure for light-induced self-writing of micropillar arrays followed by spray coating of a PTFE nanoparticle layer to attain superhydrophobic surface structures. a) Schematic of the optical setup, wherein the resin is placed in a well with a transparent material as the substrate, which rests on the photomask. The blue LED light irradiates the resin from below, after passing through the photomask and transparent substrate. The photomask consists of a 2D square array of apertures of diameter *D* and array spacing of *S*. b) Schematic of the process by which the PTFE coated micropillar arrays are fabricated. Firstly, transmission of optical beams through the resin causes self-focusing and self-trapping, whereby solid pillars begin to grow upward from the transparent substrate. Removal of the uncured monomer leaves the periodically space pillars adhered to the transparent substrate. The pillars are subsequently coated with a thin-layer of PTFE nanoparticles, specifically over the pillar tips.

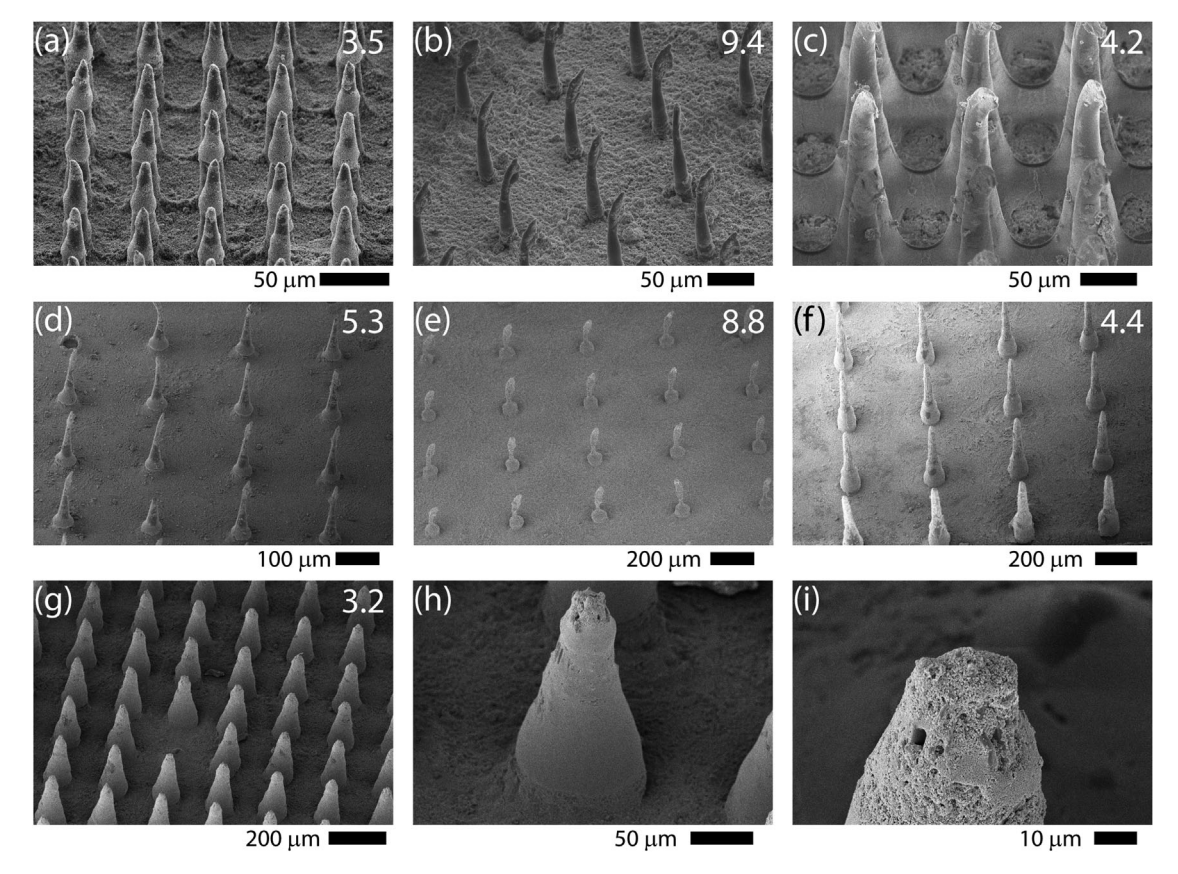


Figure 2. SEM images of the micropillar arrays produced through light-induced self-writing using photomasks a) 10/50, b) 10/100, c) 40/100, d) 40/200, e) 40/400, f) 80/400, and g) 80/200. h) Close up image of an individual pillar shown in (g). i) Close up of the tip of pillar shown in (h) revealing the PTFE nanoparticle coating. Diameters measured at mid-height are 12, 13, 28, 12, 45, 44, and 67 μm, for (a–g), respectively. Micropillar aspect ratios are provided at the top right in (a–g). All pillars are vertically aligned and stand erect over, and adhered to, the transparent substrate. The substrate itself is also coated with PTFE nanoparticles. All arrays possess square symmetry and the same array spacing as their correspond photomasks used to synthesize them. Images were captured at different viewing angles to clearly show the structure of each array.

the substrate with the same symmetry and spacing as the optical beams that generated them. The pillars do not strictly have a cylindrical "pillar"-like shape, especially at their tips, but rather are tapered along their length, and may be more precisely characterized as having a conical frustum shape or a simply a cone. This resultant shape is owing to photocuring being strongest and fastest at the center of the optical beam, as well as the continuous lensing of light at the tip, which will narrow the pillar's diameter closer to its end. Nevertheless, pillar diameters away from the tip were approximately equal to, or slightly greater, than the diameter of the aperture employed. Close up images reveal that spray coating adequately covers the pillar tips and just below the tips along the circumferential walls, as well as the underlying substrate. Nanoparticle coverage primarily over the pillar tip and its top circumferential walls is most likely due to line of sight of the particle streamlines during spray coating. [2a] While pillar growth was explored predominately on plastic surfaces, other transparent substrates (i.e., glass, etc.) are suitable to the LISW process. The pillar diameter (D), interspacing (S), and D:S ratio are generally larger than those of structures produced by lithography, for example, yet the arrays fabricated herein still demonstrate strong anti-wetting (vide infra). Figure 2 also shows calculated

micropillar aspect ratios (height:width) in the range of approximately 2.5–10 (diameter measured at the mid-height of pillars), and are typical aspect ratios produced in other works on micropillar fabrication.

Pillar heights were in the range of 70–500 µm, in which taller pillars were observed for greater aperture sizes. The pillar height also depends on the resin thickness, as revealed by pillars formed in the meniscus region near the walls of the cell (See Supporting Information, Figure S1). We exploited this dependence in order to produce micropillars of different heights for each given mask pattern, as shown in Figure 3. Each mask pattern has its own range of resin thicknesses in which individual and mechanically stable (i.e., no bending) pillars were produced. For any given mask and its respective thickness range, larger resin thicknesses resulted in tall pillars that might bend due to their self-weight (See Supporting Information, Figure S2). These taller pillars would also apparently become fused with neighboring pillars, which can be reversed when immersed in water, as observed by others. [22] On the other hand, irradiation of resins that are thinner than a mask's respective range produced small polymer "bumps" that were incompletely cured and easily removed during washing. Despite varying the resin thickness, the diameter of the pillar

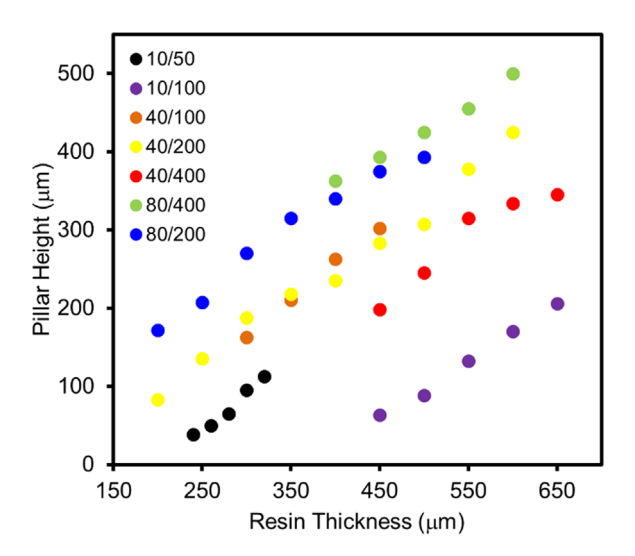


Figure 3. Plots of the resultant pillar height as a function of the resin thickness for seven different mask configurations (D/S). All plots show monotonically increasing trends with increased resin thickness and have specific resin thickness ranges in which pillars may be formed. The plots display the practical selection range of pillar heights as well as array spacing that may be fabricated using the light-induced self-writing technique. Each data point is the average over three samples (c.v. \approx 5%). Notably, all plots have approximately the sample slope (\approx 0.85), indicating predictable tuning of the pillar height with resin thickness over the entire range of masks employed.

at its base remained relatively constant, which can be explained by the confinement of light to the pillars; only the height and the relative shape changes (i.e., hemisphere, pointed, conical, conical frustum). Owing to the small optical beams and small array spacing, structures produced using the 10/50 mask had a lower and narrower resin thickness range in which practical structures were produced ($240-320\,\mu\text{m}$), below which no reliable pillars were formed, and above which the pillars were embedded in an insoluble gel. Overall, we exploited this

dependence on resin thickness (controlled by total resin volume injected into the cell) to fabricate micropillar arrays with varied heights, in order to determine the optimum for each array that achieves the best anti-wetting properties.

As the blue-light sensitizing camphorquinone is significantly consumed during the photocuring process, the surfaces show reasonable transparency. **Figure 4**a shows that within the UV/Vis/NIR region the transmittance of the micropillar arrays is between the range of 0.4 (UV region) and 0.9 (NIR). The general trend in transparency is such that pillars of smaller diameter and arrays with greater spacing yield the greatest transparency, as similarly observed in other studies. ^[23] This is associated to a greater fraction of the surface consisting of air, thereby leading to greater transmittance of light. PTFE nanoparticles generally show good transparency, ^[19] indicating that reduction in transparency might be associated to absorption or scattering by the pillars. Yet, the reasonable transparency is visually evident, as well as the apparent repellency by the surface for a water droplet (Figure 4b).

Figure 5 shows close-up images of water droplets resting on the micropillar array structures. The images confirm that the pillars trap air within their interstitial spaces, as there is no observable, significant impregnation by the liquid. Hence, wetting most likely follows a Cassie-Baxter (CB) model^[24]:

$$cos(\theta_r) = f_1 cos(\theta_s) - f_2 \tag{1}$$

where θ_r and θ_s are the water contact angles (WCAs) of the micropillar array surface and a smooth surface, respectively, and f_1 and f_2 are the fractional interfacial areas of the solid material (i.e., PTFE coating) and air in contact with a liquid droplet, respectively ($f_1 + f_2 = 1$). Micropillar arrays at this size-scale are attractive, because they allow for visual confirmation of the antiwetting properties as well as the wetting mechanism (i.e., Cassie-Baxter; or Wenzel in the case of liquid impregnation into the array). We examined the deliberate spreading of a droplet over the surface, which revealed its strong repellency to wetting (See Supporting Information, Video 1).

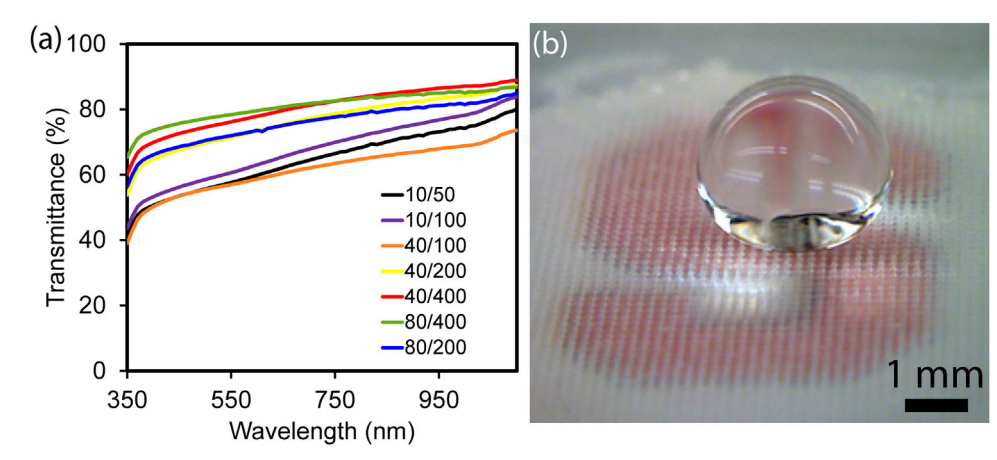


Figure 4. a) Transmittance spectra of self-written micropillar arrays. Denser arrays of pillars show reduced transmittance. All curves show a monotonic increase with increased wavelength. The sharp drop off in transmittance at smaller wavelength is associated to strong absorption by the plastic substrate. b) Photograph of a water droplet resting on a micropillar array deposited on a plastic substrate, with observable hydrophobic surface properties. Image shows wetting over a structure produced with an 80/200 mask.

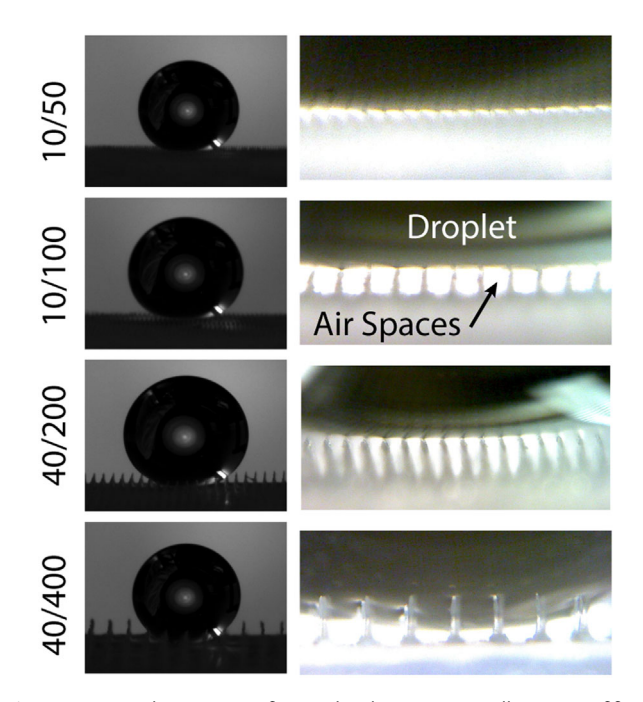


Figure 5. Exemplary images of water droplets on micropillar arrays of four different array spacing and corresponding macro-lens images zoomed in on the bottom of a droplet resting on the pillars. The water droplets visually show high surface contact angles, and the close-up images reveal that the droplets rest on the tips of the pillars, with no evidence of pillars puncturing through the air—liquid interface. It can also be observed that the pillars themselves do not yield from the weight of the droplet, thereby allowing for a trapped layer of air between the droplet and substrate underlying the micropillars, which establishes the Cassie-Baxter condition for wetting.

Figure 6 summarizes the contact angles (advancing and receding) as a function of the mask pattern. We show the greatest WCAs attained for each mask, achieved at a specific resin thickness. A full summary of contact angles and hysteresis for all micropillar arrays can be found in the Supporting Information (Table S1-S4). Remarkably, micropillar arrays over all investigated D and S values attain superhydrophobicity (WCA $> 150^{\circ}$) and low contact angle hysteresis. This shows the versatility in the selection of the pillar diameter and spacing, toward specific applications, without concern for any deleterious effect on anti-wetting. Furthermore, the high contact angle leads to very small slide-off angles of less than 10° as revealed by the immediate slipping of a droplet upon gradual tilt of the structure (Figure 7). The combination of both the micropillar arrays and the PTFE nanoparticle coating was necessary to attain superhydrophobicity, as uncoated micropillar arrays produced WCAs between 120 and 130°. There was no trend in the WCA values as a function of resin thickness, rather the WCA values fluctuated above 150° and below it, for all masks explored. One explanation for this is that the shape of the tip of the pillar varied from a rounded hemisphere-like shape to one that is very pointed, the latter of which showed the tendency to bend, indicating lower mechanical strength. We observed that all shapes that showed superhydrophobicity had flattened or hemispherical shapes. Two generous coats of PTFE were

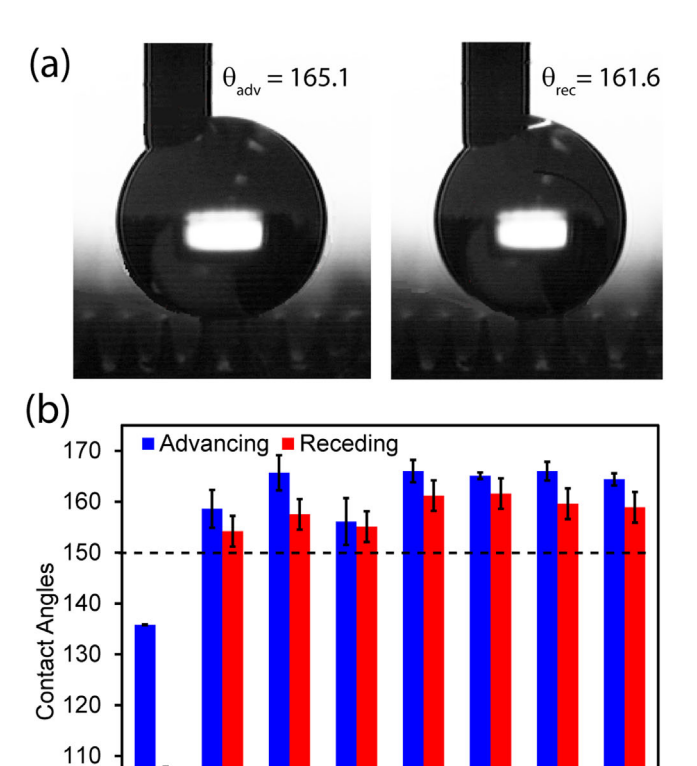


Figure 6. a) Advancing and receding contact angles of water on a micropillar array surface (40/200 mask). Both advancing and receding contact angles are well above 150°, establishing strong superhydrophobic character. The volume of the droplet is $\approx\!4.2\times10^{-3}\,\mu\text{L}$ and $\approx\!2.1\times10^{-3}\,\mu\text{L}$ for advancing and receding measurements, respectively. b) Measured advancing and receding water contact angles as a function of mask pattern. The black dashed line indicates the angles above which wetting is characteristically superhydrophobic. "No Mask" refers to a planar film of TMPTA spray coated with PTFE nanoparticles. Error bars are based on a 95% confidence interval (10 measurements). All samples show superhydrophobic character, both for advancing and receding contact angles. The close values of the advancing and receding contact angles, all of which are within the others confidence interval for each respective mask, is statistical evidence of low contact angle hysteresis (max. 4° for 10/50, min. 1° for 40/100). There is no statistically significant difference between droplet wetting on arrays produced from different masks. The wetting achieved by all structures is a significant enhancement over a planar film. Results indicate that consistent superhydrophobicity can be achieved over a range of micropillar array structures.

401200

801200

AOIAOO

801400

ADITOD

necessary to attain superhydrophobicity, via complete coverage of the pillar tips, as similarly observed with concentration variations in PTFE nanoparticle composite materials.^[25]

To confirm that the hydrophobicity of the micropillar arrays was associated to the Cassie-Baxter model for wetting, we calculated the WCA for each structure from measurements of the pillar diameter at the tip. The fractional interfacial area (f_1) may be calculated as:

100

90

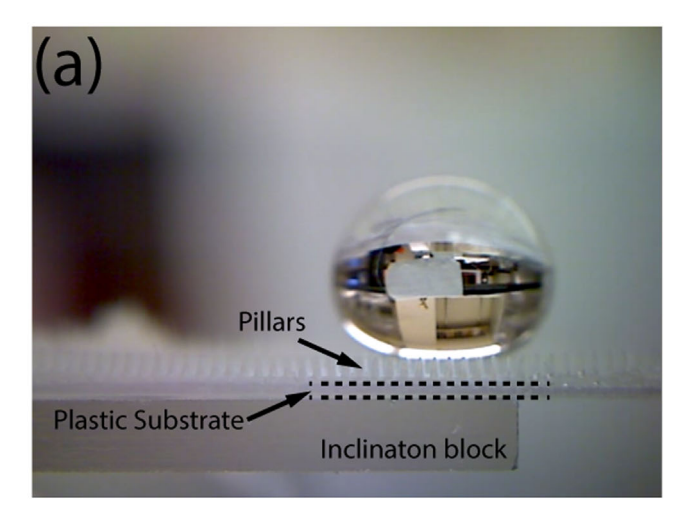




Figure 7. Visual observation and determination of the slide-off angle. a) A stationary droplet resting over a micropillar array surface (40/200 mask shown). Dotted lines demarcate the interfaces between the pillars, the plastic substrate, and the large substrate block (glass microscope slide) which was tilted to provide inclination. b) Upon a small inclination of the micropillar array substrate, the droplet immediately begins to slide over the surface. The minimum slide-off angle is $\sim 2.5^\circ$. The arrow indicates the direction of slide-off upon inclination.

$$f_1 = \frac{\pi r^2 + 2\pi rh}{S^2} \tag{2}$$

where r is the radius at the tip of the pillar, and h is the height of the wetting area below the tip. We employed macro-lens imaging of stationary droplets in equilibrium to estimate h, and SEM images to measure the radius, r. See Supporting Information for exemplary images captured to measure h (Figure S3). As pillar shape could taper down to a small point at its end, to be consistent the pillar radius used was that measured at a location of h below the pillar tip. This model approximates the micropillar tip with a cylindrical shape. See Supporting Information for measured values (Table S5). The calculated WCAs based on the Cassie–Baxter model show good agreement with the observed static WCAs (See Table S6, S7 and Figure S4). Discrepancies between measured and calculated WCAs are associated to the

accuracy of measuring the pillar tip shape, the value of h, as well as assumptions of the model; namely, the tip shape could be more closely modeled as a conical frustum. Nevertheless, the shape model is demonstrably sufficient to confirm the Cassie-Baxter mechanism for wetting.

The micropillar array structures were durable, as evidenced by their capability to retain their superhydrophobicity (and structure) after the application of moderate compressive stresses both over the entire surface and also locally (See Supporting Information, Figure S5, Video 2 & 3). No observable, significant damage was caused through the application of stress to the surface.

3. Discussion

The conical shape, which naturally forms with self-writing, is quite beneficial to superhydrophobicity. Experiments and calculations on a wide range of surface topographies suggest enhancement of superhydrophobicity with dense arrays of conical or pyramidal structures with small hemispherical caps. [26] Consistent with our results, this structure produces a Cassie-Baxter state with higher apparent contact angles and lower contact angle hysteresis, owing to the smaller contact area between the pillars and the liquid, as well as negligible contact line pinning by the hemispherical tops. Based on our results, we can make the following comparisons to previous works on conically shaped pillars employed for superhydrophobicity and transparency. The transmission of our samples is more uniform over the visible light spectrum, as compared to interference effects observed from low aspect ratio pillars with silica nanoparticle coated tips[2b] and nano-textured silica surfaces, [27] albeit our samples show lower transmittance values. As compared to the structures produced from polydimethylsiloxane, [28] we sustained contact angles greater than 150 over our structure variations, yet we attain lower transmittance values. Higher transmittances may be achieved in our materials by spray-coating with other nanoparticle materials, such as silica, or by employing high optically transparent resins. Lastly, the contact angles attained herein are in some instances greater than those produce from silicon structures.^[29]

Pillar growth entails a combination of light-induced selfwriting and the presence of oxygen inhibition (owing to ambient air exposure) to free-radical polymerization, as we have described previously.[16] Namely, oxygen can permeate into the resin, thereby inhibiting growth everywhere except in regions with intense light exposure. Hence, inhibition is strong in the regions between the optical beams, as well as in proximity to the resin-air interface. Such regions are commonly referred to as "dead zones", whose presence enables high resolution pattern formation, critical to 3D writing and microfabrication.^[30] Likewise, this effect is critical to the formation of individual pillars. We found that the resin underwent complete crosslinking (i.e., gelation) when the experimental cells were sealed (i.e., closed to ambient air), or that the pillars, if any, were embedded in a highly viscous gel that was difficult to remove by washing. Whereas, by using a cell open to the ambient environment, the resin is provided with a continuous supply of oxygen, such that individual pillars can form with negligible photocuring in the interstices.

www.advancedsciencenews.com

By increasing the resin height, the dead zone at the resin-air

interface is moved upward and away from the entrance location

of the optical beams, and the pillars can grow taller within the same amount of time and at the same exposure intensity.

Changing the pillar height via the volume of resin injected into

the cell is quite beneficial, because resin volumes can be easily

controlled. Inhibition can also explain why pillar formation in

very thin resins might not completely solidify (i.e., attain

sufficient crosslinking), owing to the slower, or even completely

arrested, photopolymerization reaction. At very large resin

thicknesses, oxygen is unable to significantly permeate through

the entire resin depth, resulting in pillars trapped in a gel formed

in their interstices. Or, the pillars grow to a height such that they

easily bend and, consequently, reliable anti-wetting properties

may not be expected (and were not explored herein). This

explains the minimum and maximum resin heights within

which high-quality micropillar arrays are achieved. This range

changes with the size and spacing of the optical beams, because

both parameters change the irradiation conditions in terms of

overall exposure, radicals generated, and proximity of the beams

(i.e., for radical diffusion). Pillar growth is predominately along

the optical beams' long axis; however, there always exists some

photoinitiation at its lateral peripheries, which enables the pillars

to attain a slightly greater diameter than dictated by the mask's

apertures. Yet, based on pillar measurements, the diameter

(away from the pillar tip) is precisely defined by the aperture.

With a smaller spacing desired between pillars, care must be

taken in selecting an aperture size to account for the resultant, slightly larger diameter pillars, lest they come into contact with

It is notable that such large pillars and large pillar inter-

spacing in these arrays lead to superhydrophobic properties.

Common pillar sizes from lithography are <10 μm with spacing

no larger than $\approx 50 \,\mu\text{m}$, with better properties observed with

finer spacing to ensure reliable trapping of air to attain the

Cassie-Baxter state that leads to superhydrophobicity. It is

probable that the crosslinked structure and the wider diameters

of the pillars herein allow them to attain greater mechanical stiffness, such that less pillars, spaced further apart, can retain

their nearest neighbors during their lateral growth.

www.aem-iournal.com

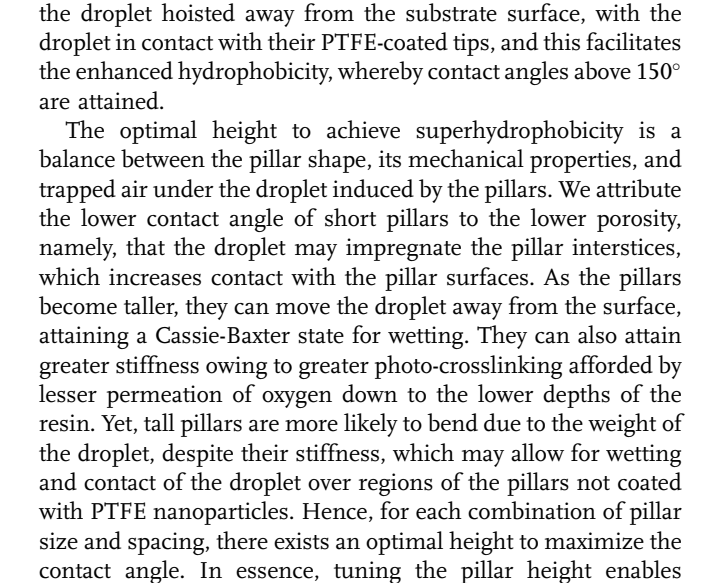
tunable air trapping, which can change the surface wetting properties.^[31] The tapered shape common among all pillars fabricated herein is beneficial in that it reduces the solid interfacial fraction in contact with the droplet, which can

increase the contact angle.

The fluctuations in the WCA with pillar height (controlled by resin thickness) can be explained by the shape of the pillar tip, which depends on its growth over time. The shape most likely oscillates between a round lens, which focuses the beam, and a sharp pointed tip, which forms from the focused beam and then eventually rounds off to begin this cyclic process once more (Figure 8). As this process occurs as the pillar height is increasing, variation of the resin thickness stops pillar growth when the tip is one of either of these shapes. The rounded shape most likely leads to better anti-wetting, because it is less likely to bend and allow more contact area with the pillars, which would decrease the contact angle. The evolution of the shape of the pillar tip over the course of growth is the subject of current study.

From the results, we can draw a few principles on engineering the structures with LISW to attain superhydrophobicity. For a fixed diameter, *D*, change of the spacing, *S*, allows different areal fractions and air trapping conditions, and sparser arrays (greater *S*) need to be taller to allow for the droplet to be raised away from the surface. For a fixed spacing, a greater diameter yields pillars that are mechanically more rigid, and thus can be taller and still yield anti-wetting with less likelihood of bending. We found no conclusive correlation between the optimal resin thickness and the mask parameters, rather a range of resin thicknesses should be explored for a desired mask in order to find the optimum for anti-wetting. Nevertheless, our results show that superhydrophobicity is attainable over a range of micropillar interspacings and typical micropillar diameters.

The light-induced self-writing approach is straightforward, only a mask and light source are required to transform a resin into a micropillar array structure. The process is notable for its short duration to produce the final structure: a total of $\approx 30 \, \text{min}$ of growth (irradiation + spray coating) combined with ancillary wash steps. In terms of the technique, self-writing is versatile in that a range of pillar sizes, spacings, and symmetries can be



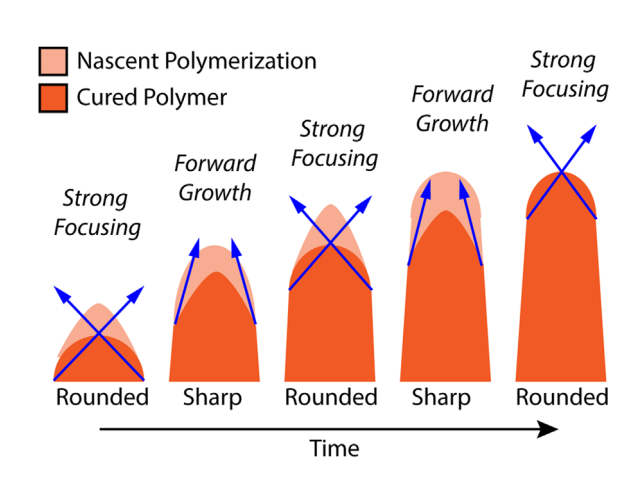


Figure 8. Proposed mechanism for the oscillation of the micropillar tip shape caused by strong focusing, followed by consequent growth, and the repetition of these two processes.



www.advancedsciencenews.com

www.aem-iournal.com

ADVANCED ENGINEERING MATERIALS

fabricated. Self-writing studies place the smallest pillar diameter down to 1 μ m,[12a] opening opportunities for surface roughness at finer scales. While we irradiate from below and through a transparent substrate, the LISW technique can be employed for depositing on opaque surfaces by irradiating the resin from above. Irradiation of a resin open to the ambient environment is attractive, especially for large-scale coatings in which enclosure of the intended substrate or object to be coated is neither practical, nor feasible. Furthermore, the inherent fiber optic properties of the pillars make them attractive for optical applications, such as synthetic eyes. $^{[11,32]}$ Hence, we have also demonstrated a versatile approach for designing functional surface architectures.

4. Conclusion

In summary, we have shown a new two-step approach to fabricate micropillar arrays on transparent surfaces and to impart anti-wetting properties. The process combines a visiblelight sensitized resin with light-induced self-writing to fabricate a multitude of periodically spaced micropillars, which can be subsequently coated with nanoparticles toward surface functionality. The pillar diameter and inter-spacing can be tuned via photomask design. All micropillar arrays yield superhydrophobic surface properties and low contact angle hysteresis. The significance of this work is the capability to prototype micropillar array structures using visible light photocuring, and whose structure is straightforwardly tuned and superhydrophobic properties easily achieved. The results indicate that this approach is a potential platform for creating and designing micropillar array surface structures for applications in which they play a critical role.

5. Experimental Section

Materials: Trimethylolpropane triacrylate (TMPTA) and polytetrafluoroethylene (Teflon, PTFE) nanoparticles (200–300 nm) were purchased from Sigma-Aldrich. The visible-light photoinitiator system consisted of free-radical initiator camphorquinone (CQ) purchased from Sigma Aldrich, and cationic initiator (4-octyloxyphenyl) phenyliodonium hexafluoroantimonate (OPPI) purchased from Hampford Research Inc. All chemicals were used as received.

Photopolymer Preparation: Photocurable resins (liquid at room temperature) were prepared by mixing TMPTA with CQ (2.5 wt% of total mixture) and OPPI (1.5 wt% of total mixture). Mixtures were continuously stirred for 24 h, while protected from exposure to ambient light. CQ sensitizes the photoreactive blend to blue light ($\lambda_{max} = \approx 470$ nm), initiates the free-radical polymerization of TMPTA, and facilitates free-radical decomposition of OPPI which accelerates photopolymerization. [33]

Photocuring: The resin was poured into an open cell consisting of a Teflon ring placed on top of a transparent plastic substrate. The thickness of the resin in the cell was measured by a custom-made device, which contained a linear translation stage, a tip, and a camera. The bottom and top position of the film were recorded as the tip touched one of them, and aliquots of the mixture were added to the cell until the desired thickness was achieved. We measured the film thickness at the center of cells to avoid resin film distortion at the cell edges due to the meniscus. The resin was irradiated from below with collimated blue LED light ($\lambda_{max} = 470 \, \text{nm}$, Thorlabs Inc.) at an exposure intensity of $10 \, \text{mW cm}^{-2}$ for $20 \, \text{min}$. The peak emission wavelength of the LED corresponds to the peak absorbance of CQ, which maximizes photon

absorbance. To generate a periodic array of optical beams, the LED light was first passed through a photomask (Photosciences Inc.) that consisted of a square array of circular apertures of diameter D and spacing of S. Mask patterns are expressed herein as a D:S ratio (in microns). This optical beam array was subsequently transmitted through the resin. Aperture diameters explored were 10, 40, and $80\,\mu m$, and interspacings of 50, 100, 200, and $400\,\mu m$. Typical resin thicknesses explored were between 200 and $650\,\mu m$, with the exception of the 10/50 mask for which resin thicknesses were $240-320\,\mu m$. After irradiation, the mixture was washed three times with ethanol to remove excess unreacted monomer. The samples were then dried in a vacuum oven at $50\,^{\circ}\text{C}$ for 3 h to remove any residual solvent.

Surface Coating: The microporous surfaces were coated with a thin layer of PTFE nanoparticles using a commercial spray coater. The coating mixture consisted of PTFE nanoparticles (5 wt%) dispersed in ethanol through ultra-sonication for 5 min. Spray coating was applied over the samples using nitrogen as the carrier gas and an applied flow pressure of 40 psi. Two generous coats, with ambient drying in between, was sufficient to confer a thin coating, particularly over the top regions of the pillars. As a control and for comparison, a uniform (i.e., planar) film of TMPTA was also spray coated with a thin layer of PTFE nanoparticles.

Imaging: The micropillar arrays were imaged with an optical microscope (Zeiss Axioscope) equipped with a camera (Axiocam 105). Photographs and videos of the micropillar array surface and droplet wetting were captured with a digital microscope (MicroView), for which we refer to as macro-lens images. Scanning electron microscopy (SEM) images were attained using a JEOL JSM-5600 at an acceleration voltage of 5 keV. SEM samples were sputtered with a thin metal layer prior to imaging.

Wettability Measurements: Advancing and receding contact angle measurements were collected using a VCA Optima system (AST Products). Measurements on droplets were collected with a manually operated syringe to increase or decrease the volume of the droplet, in order to determine the advancing and receding contact angles, respectively, which were measured by the system. Static contact angle measurements were performed via the sessile drop method using Ramé-Hart 250 F1 contact angle goniometer. A water droplet was placed onto the substrate, and a circular drop profile from the camera was used to determine the contact angles using DROP Image Advanced software.

Durability Tests: Simple durability testing was performed by the application of a compressive stress on a micropillar array using the weight of a 67.15 g cylindrical (13 mm diameter) steel block. The contact area between the block and the micropillar array was calculated to be approximately 0.4 mm², based on the average tip area of the pillars and the number of pillars within the block's area. The total pressure over all tip surfaces combined was approximately 1.645 MPa, while on an individual pillar it was 495.8 Pa. In an alternate test, the weight of the block was applied using the edge of a coin (US quarter), which was pressed down onto the surface to provide a more concentrated and thus greater stress. The micropillar array structure as well as the spreading of a water droplet over the surface was observed both before and after the application of the stress.

Acknowledgements

The authors gratefully acknowledge funding supported by the American Chemical Society under the grant agreement number PRF# 57332-DNI7, the National Science Foundation under grant number CMMI-1751621, as well as support from the College of Engineering and Computer Science at Syracuse University.

Supporting Information

Supporting Information is available from the Wiley Online Library or from the author.



www.advancedsciencenews.com

www.aem-iournal.com

Conflict of Interest

The authors declare no conflict of interest.

Keywords

hydrophobicity, light-induced self-writing, micropillars, nanoparticles, re-entrant

Received: October 30, 2018 Revised: December 9, 2018 Published online:

- a) Y. M. Zheng, D. Han, J. Zhai, L. Jiang, Appl. Phys. Lett. 2008, 92, 084106;
 b) K. Koch, B. Bhushan, W. Barthlott, Prog. Mater. Sci. 2009, 54, 137;
 c) M. J. Liu, S. T. Wang, Z. X. Wei, Y. L. Song, L. Jiang, Adv. Mater. 2009, 21, 665.
- [2] a) K. Golovin, D. H. Lee, J. M. Mabry, A. Tuteja, Angew. Chem. Int. Ed. 2013, 52, 13007; b) S. Y. Lee, Y. Rahmawan, S. Yang, ACS Appl. Mater. Interfaces 2015, 7, 24197.
- [3] C. M. Chen, S. Yang, Adv. Mater. 2014, 26, 1283.
- [4] W. W. Shi, L. Wang, Z. Y. Guo, Y. M. Zheng, Adv. Mater. Interfaces 2015, 2, 1500352.
- [5] M. J. Kreder, J. Alvarenga, P. Kim, J. Aizenberg, Nat. Rev. Mater. 2016, 1, 15003.
- [6] K. Golovin, M. Boban, J. M. Mabry, A. Tuteja, ACS Appl. Mater. Interfaces 2017, 9, 11212.
- [7] Y. Wang, X. M. Li, H. M. Tian, H. Hu, Y. Tian, J. Y. Shao, Y. C. Ding, J. R. Soc. Interface 2015, 12, 20150090.
- [8] R. Ras, A. Marmur, RSC Soft Matter Ser. 2017, 5, V.
- [9] H. B. Zhang, C. Bian, J. K. Jackson, F. Khademolhosseini, H. M. Burt, M. Chiao, ACS Appl. Mater. Interfaces 2014, 6, 9126.
- [10] a) Z. Q. Fan, W. J. Zhang, Y. L. Fu, L. Q. Yan, X. B. Ma, J. Phys. Chem. C 2016, 120, 6824; b) K. Miller, M. X. Li, K. M. Walsh, X. A. Fu, J. Micromech. Microeng. 2013, 23, 035039;
- [11] B. M. Jun, F. Serra, Y. Xia, H. S. Kang, S. Yang, ACS Appl. Mater. Interfaces 2016, 8, 30671.
- [12] a) A. S. Kewitsch, A. Yariv, Opt. Lett. 1996, 21, 24; b) A. S. Kewitsch,
 A. Yariv, Appl. Phys. Lett. 1996, 68, 455; c) M. Kagami, T. Yamashita,
 H. Ito, Appl. Phys. Lett. 2001, 79, 1079.
- [13] S. Shoji, S. Kawata, A. A. Sukhorukov, Y. S. Kivshar, Opt. Lett. 2002, 27, 185.

- [14] S. Shoji, S. Kawata, Appl. Phys. Lett. 1999, 75, 737.
- [15] a) A. J. Jacobsen, W. Barvosa-Carter, S. Nutt, Adv. Mater. 2007, 19, 3892; b) T. Yamashita, M. Kagami, H. Ito, J. Lightwave Technol. 2002, 20, 1556.
- [16] F. H. Chen, S. Pathreeker, S. Biria, I. D. Hosein, *Macromolecules* 2017, 50, 5767.
- [17] a) A. J. Jacobsen, W. Barvosa-Carter, S. Nutt, Acta Mater. 2008, 56, 2540; b) A. J. Jacobsen, W. B. Barvosa-Carter, Google Patents, HRL Laboratories LLC, 2012; c) H. Nanthakumar, F.-H. Chen, S. Biria, I. D. Hosein, Results Phys. 2017, 7, 2194.
- [18] a) S. Biria, P. P. A. Malley, T. F. Kahan, I. D. Hosein, J. Phys. Chem. C
 2016, 120, 4517; b) I. D. Hosein, H. Lin, M. R. Ponte, D. Basker, K. Saravanamuttu, Org. Photonic Mater. Dev. Xvi 2014, 8983, 89830E; c) I. B. Burgess, M. R. Ponte, K. Saravanamuttu, J. Mater. Chem.
 2008, 18, 4133; d) K. Kasala, K. Saravanamuttu, J. Mater. Chem. 2012, 22, 12281; e) M. R. Ponte, R. Welch, K. Saravanamuttu, Opt. Express 2013, 21, 4205.
- [19] A. Y. Zhuang, R. J. Liao, S. C. Dixon, Y. Lu, S. Sathasivam, I. P. Parkin, C. J. Carmalt, RSC Adv. 2017, 7, 29275.
- [20] S. Biria, I. D. Hosein, ACS Appl. Mater. Interfaces 2018, 10, 3094.
- [21] a) S. Biria, I. D. Hosein, Macromolecules 2017, 50, 3617; b) S. Biria, P. P. A. Malley, T. F. Kahan, I. D. Hosein, ACS Macro Lett. 2016, 5, 1237.
- [22] D. Chandra, S. Yang, Acc. Chem. Res. 2010, 43, 1080.
- [23] S. M. Kang, S. M. Kim, H. N. Kim, M. K. Kwak, D. H. Tahk, K. Y. Suh, Soft Matter 2012, 8, 8563.
- [24] A. B. D. Cassie, S. Baxter, Trans. Faraday Soc. 1944, 40, 0546.
- [25] A. Tropmann, L. Tanguy, P. Koltay, R. Zengerle, L. Riegger, Langmuir 2012. 28, 8292.
- [26] M. Nosonovsky, B. Bhushan, Microsyst. Technol. 2005, 11, 535.
- 27] K. C. Park, H. J. Choi, C. H. Chang, R. E. Cohen, G. H. McKinley, G. Barbastathis, ACS Nano 2012, 6, 3789.
- [28] C. V. Ngo, G. Davaasuren, H. S. Oh, D. M. Chun, Int. J. Precis. Eng. Manuf. 2015, 16, 1347.
- [29] V. Zorba, E. Stratakis, M. Barberoglou, E. Spanakis, P. Tzanetakis, S. H. Anastasiadis, C. Fotakis, Adv. Mater. 2008, 20, 4049.
- [30] a) D. Dendukuri, P. Panda, R. Haghgooie, J. M. Kim, T. A. Hatton, P. S. Doyle, *Macromolecules* 2008, 41, 8547; b) J. R. Tumbleston, D. Shirvanyants, N. Ermoshkin, R. Janusziewicz, A. R. Johnson, D. Kelly, K. Chen, R. Pinschmidt, J. P. Rolland, A. Ermoshkin, E. T. Samulski, J. M. DeSimone, *Science* 2015, 347, 1349.
- [31] Y. Zhang, S. Sundararajan, J. Micromech. Microeng. 2008, 18, 035024.
- [32] I. D. Hosein, H. Lin, M. R. Ponte, D. K. Basker, M. A. Brook, K. Saravanamuttu, Adv. Funct. Mater. 2017, 27, 1702242.
- [33] J. V. Crivello, J. Polym. Sci. A Polym. Chem. 2007, 45, 3759.